










RESEARCH ARTICLE | MARCH 17 2023

The role of boron related defects in limiting charge carrier lifetime in 4H-SiC epitaxial layers

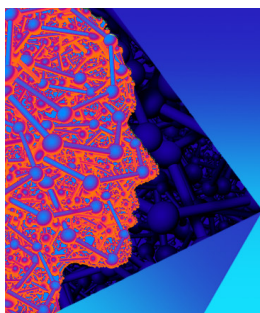
Misagh Ghezellou ; Piyush Kumar ; Marianne E. Bathen ; Robert Karsthoﬀ ; Einar Ö. Sveinbjörnsson ; Ulrike Grossner ; J. Peder Bergman ; Lasse Vines ; Jawad Ul-Hassan 



APL Mater. 11, 031107 (2023)
<https://doi.org/10.1063/5.0142415>



CrossMark



APL Materials
 Special Topic: 2D Materials
 for Biomedical Applications

Submit Today



The role of boron related defects in limiting charge carrier lifetime in 4H-SiC epitaxial layers

Cite as: APL Mater. 11, 031107 (2023); doi: 10.1063/5.0142415
Submitted: 13 January 2023 • Accepted: 27 February 2023 •
Published Online: 17 March 2023



Misagh Ghezellou,^{1,a)} Piyush Kumar,² Marianne E. Bathen,² Robert Karsthof,³
Einar Ö. Sveinbjörnsson,^{1,4} Ulrike Grossner,² J. Peder Bergman,¹ Lasse Vines,³
and Jawad Ul-Hassan¹

AFFILIATIONS

¹ Department of Physics, Chemistry, and Biology (IFM), Linköping University, SE-581 83 Linköping, Sweden

² Advanced Power Semiconductor Laboratory, ETH Zürich, 8092 Zürich, Switzerland

³ Department of Physics, University of Oslo, 0316 Oslo, Norway

⁴ Science Institute, University of Iceland, IS-107 Reykjavík, Iceland

^{a)} Authors to whom correspondence should be addressed: Misagh.Ghezellou@liu.se and Jawad.Ul-Hassan@liu.se

ABSTRACT

One of the main challenges in realizing 4H-SiC (silicon carbide)-based bipolar devices is the improvement of minority carrier lifetime in as-grown epitaxial layers. Although $Z_{1/2}$ has been identified as the dominant carrier lifetime limiting defect, we report on B-related centers being another dominant source of recombination and acting as lifetime limiting defects in 4H-SiC epitaxial layers. Combining time-resolved photoluminescence (TRPL) measurement in near band edge emission and 530 nm, deep level transient spectroscopy, and minority carrier transient spectroscopy (MCTS), it was found that B related deep levels in the lower half of the bandgap are responsible for killing the minority carriers in n-type, 4H-SiC epitaxial layers when the concentration of $Z_{1/2}$ is already low. The impact of these centers on the charge carrier dynamics is investigated by correlating the MCTS results with temperature-dependent TRPL decay measurements. It is shown that the influence of shallow B acceptors on the minority carrier lifetime becomes neutralized at temperatures above ~ 422 K. Instead, the deep B related acceptor level, known as the D-center, remains active until temperatures above ~ 570 K. Moreover, a correlation between the deep level concentrations, minority carrier lifetimes, and growth parameters indicates that intentional nitrogen doping hinders the formation of deep B acceptor levels. Furthermore, tuning growth parameters, including growth temperature and C/Si ratio, is shown to be crucial for improving the minority carrier lifetime in as-grown 4H-SiC epitaxial layers.

© 2023 Author(s). All article content, except where otherwise noted, is licensed under a Creative Commons Attribution (CC BY) license (<http://creativecommons.org/licenses/by/4.0/>). <https://doi.org/10.1063/5.0142415>

I. INTRODUCTION

Silicon carbide (SiC) is a wide bandgap semiconductor with promising applications for high power, high temperature, high-frequency electronic devices. It has high thermal conductivity, critical electric field strength, and saturation drift velocity compared to conventional semiconductors (i.e., silicon). 4H-SiC, high-power microwave, high voltage switching devices have been recognized as innovative building blocks of the technologies for the green future.¹ Through these innovations, 4H-SiC, medium voltage, unipolar devices, such as Schottky barrier diodes (SBDs) and MOSFETs, have been commercialized by several manufacturers and have shown great success in power loss reduction in many power systems.² However, the specific on-resistance of power MOSFETs increases with

increasing blocking voltage ($R_{on} \propto V_B^{2.2-2.5}$) and further increases at elevated temperatures due to the mobility drop.³ 4H-SiC bipolar devices are promising to overcome these issues. By considering the conductivity modulation effect, the resistance of the thick voltage-blocking layer could be significantly reduced, and the on-resistance shows very low temperature dependency. Thus, ultra-high power devices, capable of operating at high temperatures, could be realized. However, some critical challenges in commercializing such products include the growth of thick layers through fast epitaxial growth, reduction of extended defects, improved minority carrier lifetime, surface passivation, and packaging.

High-power devices usually require thick epitaxial layers. Accordingly, fast growth rates are necessary to reduce epitaxial layer costs. In this regard, growth rates up to $100 \mu\text{m h}^{-1}$ have been

realized by implementing chloride-based chemistry, using either chloride-based precursors or HCl.^{4–7} As the standard substrate is with a 4° off-cut, extended defects in extremely thick epitaxial layers lead to a significant reduction in the yield.⁸ However, with the optimization of the growth parameters and maintenance of the reaction chamber, the formation of extended defects may be suppressed.^{9,10} From the material growth point of view, charge carrier lifetime is another parameter that needs to be appropriately optimized, as it limits the carrier concentration that can be injected for the conductivity modulation.¹¹ Surface passivation and packaging are additional challenges that need to be taken care of during post-growth processes.^{12,13}

In this study, our primary focus has been on improving the minority carrier lifetime and investigating the main lifetime limiting defects in as-grown epitaxial layers. Extensive studies have been performed to find the origin of lifetime limiting defects and to improve carrier lifetime in as-grown epitaxial layers.^{14–18} Although local carrier lifetime reduction is observed around extended defects and dislocations,¹⁹ point defects present in 4H-SiC epitaxial layers are considered to be the main lifetime limiting defects.²⁰ Among various point defects observed in the 4H-SiC lattice, the $Z_{1/2}$ center has commonly been identified as the dominant lifetime killer.^{20,21} The responsible defect introduces deep energy levels in the 4H-SiC bandgap and acts as an effective trapping or recombination center for free charge carriers. Theoretical results and comparative studies using deep level transient spectroscopy (DLTS) and electron paramagnetic resonance (EPR) revealed that the $Z_{1/2}$ center originates from the (0/2-) double acceptor transition of the carbon vacancy (V_C) in the 4H-SiC lattice.²² The V_C also gives rise to a second deep level, named $EH_{6/7}$, near mid gap and assigned to the (2+/+/0) donor transition.²² It is shown that adjusting the growth parameters, such as growth temperature and C/Si ratio, significantly affects the $Z_{1/2}$ concentration and, hence, the measured charge carrier lifetime.²³ In addition, post-growth approaches such as implantation, thermal oxidation, and annealing with a carbon cap have been shown to reduce the density of this center in epitaxial layers.^{18,24,25}

Using time-resolved photoluminescence (TRPL), we have observed relatively long minority carrier lifetimes in the samples grown through optimized growth conditions. Although the charge carrier lifetime is above 1 μ s in all epitaxial layers, a wide spread is observed in the measured values across the different samples. Interestingly, no correlation is observed among different samples between the measured carrier lifetime and the concentration of the $Z_{1/2}$ defect. Instead, temperature-dependent TRPL and minority carrier transient spectroscopy (MCTS) demonstrate a clear correlation between the measured carrier lifetimes and B-related impurities in the epitaxial layers. Furthermore, the influence of growth conditions upon the B impurity incorporation is also studied, to suppress the formation of B-related defects during growth and to achieve long charge carrier lifetimes in as-grown, 4H-SiC epitaxial layers.

II. EXPERIMENTAL

25 μ m thick, n-type, 4H-SiC epitaxial layers were grown in a horizontal, hot-wall CVD reactor on n+ substrates—all from a 150 mm wafer with a 4° off-cut toward the [11 $\bar{2}$ 0] direction. The reactor is equipped with a TaC-coated susceptor and gas foil rotation. Trichlorosilane (TCS) and methane, highly diluted in H₂,

TABLE I. Growth parameters for the studied epitaxial layers labeled C, D, F, and L.

Sample ID	Growth temperature (°C)	C/Si
C	1640	1.2
D	1600	1.05
F	1640	1.1
L	1640	1.3

were used as sources of Si and C, respectively. For intentional n-type doping, molecular nitrogen gas (N₂) was introduced into the reactor during the growth process. In the case of unintentionally doped samples, the residual background nitrogen inside the reactor is responsible for the n-type doping. The epitaxial layers were grown under different temperatures, C/Si ratios, and intentional N₂ doping, while the rest of the growth conditions were kept constant. The main growth parameters of the studied samples are summarized in Table I. The growth rate was set to 25 μ m h⁻¹ for all samples, while the change in the C/Si ratio is provided by adjusting only the methane flow rates. Notably, the studied samples are considered representative of a larger set comprising more than 25 samples.

Mercury probe station capacitance-voltage (CV) measurements were used to extract the net doping concentrations ($N_D - N_A$). Low-injection TRPL measurements were carried out in a setup equipped with a 355-nm-wavelength, pulsed (1.1 ns, 10 kHz) Nd:YAG laser for carrier excitation and a Hamamatsu photomultiplier tube (PMT) for the detection of luminescence decay. A neutral density (ND) filter and a diaphragm were placed in the beam path before the sample to tune the injection level. The near band-edge (NBE) luminescence around 390 nm was selected using a bandpass filter centered at 390 \pm 2 nm (FWHM: 10 \pm 2 nm). Another bandpass filter centered at 530 \pm 2 nm (FWHM: 10 \pm 2 nm) was also used to measure the green luminescence decay curves. Temperature-dependent TRPL measurements were performed under atmospheric ambient, where the samples were placed on a hot stage, and the temperature was measured through a thermocouple under the sample.

For electrical measurements, nickel (Ni) Schottky barrier diodes (SBDs) were formed on the epitaxial layers using thermal evaporation through a shadow mask. To facilitate probing of minority carriers, semi-transparent Schottky contacts are necessary, and were fabricated in a two-layer structure consisting of a lower layer of 600 or 900 μ m diameter and \sim 10 nm thickness, and a top layer having 300 μ m diameter and 100 nm thickness. The backside Ohmic contact was formed using silver paste.

The DLTS measurements to extract the $Z_{1/2}$ concentration were performed using a Boonton-7200, high-precision capacitance meter

TABLE II. Measured net doping concentration and minority carrier lifetime in studied samples.

Sample ID	Intentionally doped		Unintentionally doped	
	C	L	D	F
Net doping (cm ⁻³)	1.8×10^{14}	5.3×10^{13}	1.5×10^{14}	5.6×10^{13}
Carrier lifetime (μ s)	2.7	1.9	1.0	1.2

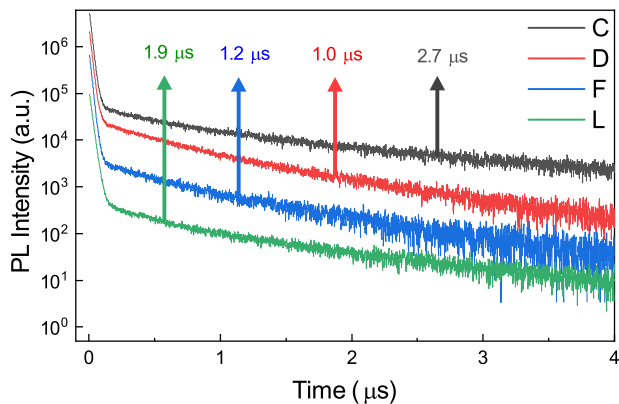


FIG. 1. RT TRPL decay curves and each sample's extracted decay constants (carrier lifetime).

operating at a test frequency of 1 MHz, in combination with an Agilent 81110A pulse generator, at a reverse bias of -10 V and pulse voltages of 10 V, using a time window of 640 ms, and in a temperature range between 20 and 320 K.

The MCTS measurements to study B-related defects were carried out at a reverse bias of -5 V and optical pulse width of 100 ms. The optical injection was induced by a 200 mW, 365 nm LED. The

measurement was performed in a temperature range 20–600 K, and the MCTS signal was then extracted from the averaged transient over ~ 10 measurements at each temperature. A Fourier transform of the recorded transients was performed using up to 28 correlation functions. The MCTS signal shown in the rest of the paper refers to the coefficient of the sine term (b1) in the Fourier series of the deep level/minority carrier transient Fourier spectroscopy (DLTFS/MCTFS).²⁶

III. RESULTS

A. Low-injection level minority carrier lifetime

The samples are split into two groups based on whether they were grown through intentional or unintentional nitrogen doping. Samples C and L are intentionally doped, whereas samples D and F are unintentionally doped. The measured values of the net doping concentration and room temperature (RT) minority carrier lifetimes are given in Table II.

The NBE TRPL decay curves are depicted in Fig. 1, where different offsets are put toward the PL intensity axis to ease the comparison (applied to all TRPL curves shown in this study). Each TRPL decay curve has two components, a high-speed component at the beginning, followed by a slow component. The fast component, usually observed at the beginning of the decay, is reported to contain a contribution from surface recombination, substrate emission, and

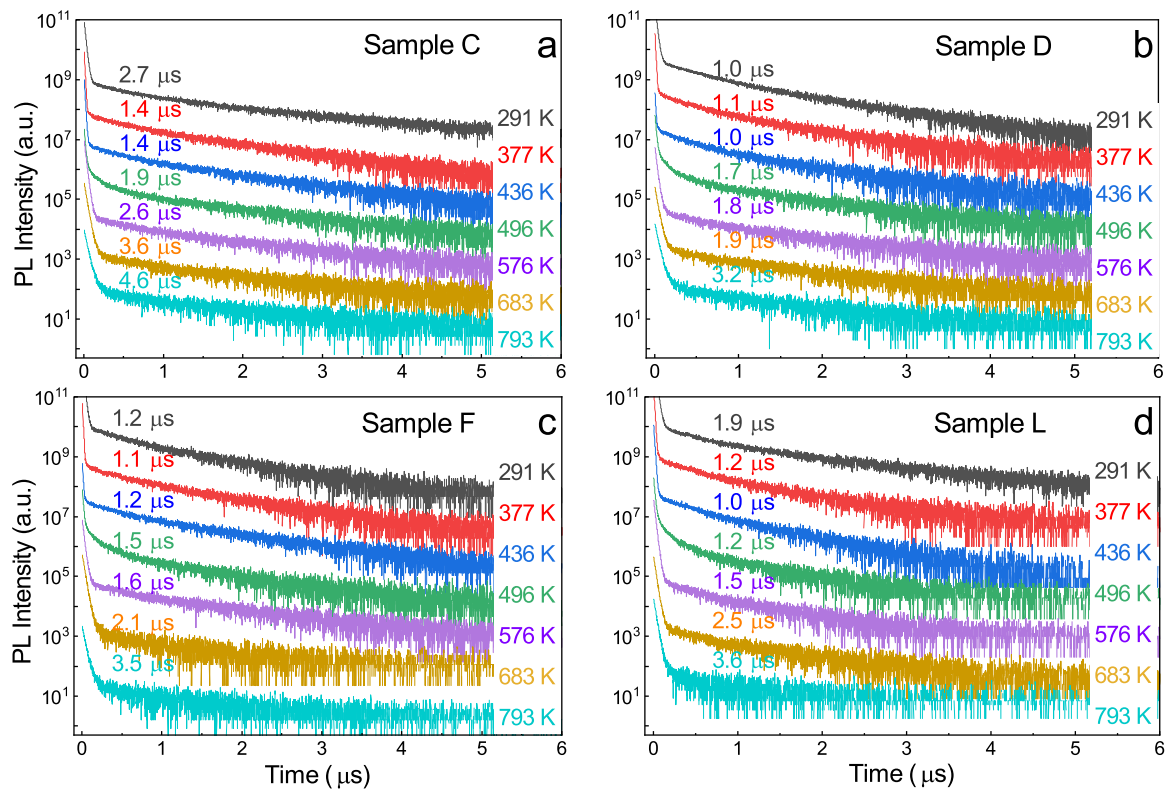


FIG. 2. TRPL decay curves and extracted decay constants, measured at different temperatures, for samples (a) C, (b) D, (c) F, and (d) L.

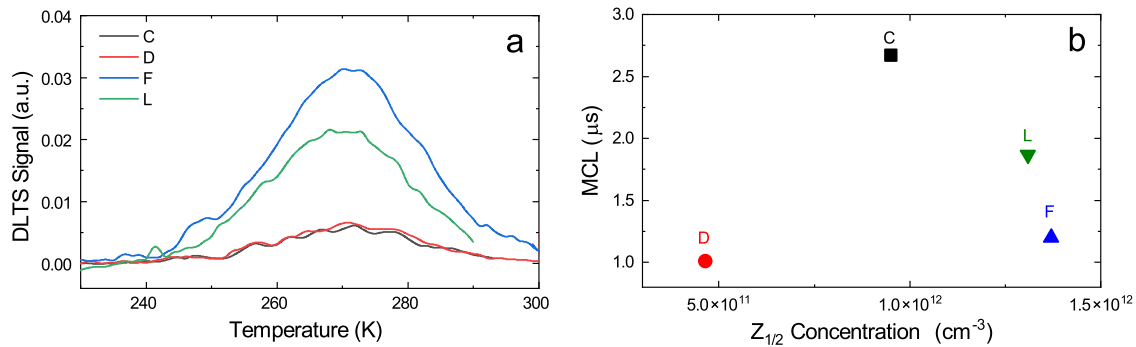


FIG. 3. (a) DLTS measurements over a temperature range 230–300 K, showing relative intensities of the $Z_{1/2}$ peak in different samples. (b) Measured carrier lifetime vs extracted $Z_{1/2}$ concentrations for the samples.

some background radiation.²⁷ The carrier lifetimes were extracted by exponential fitting on the linear part of the slow decay component of the curves, recorded under low-injection conditions. Importantly, the surface recombination velocity (SRV) is highly dependent on the surface roughness. Therefore, to ensure that the effect of SRV on the minority carrier lifetime is similar in all samples, the surface roughness values of all samples were measured by atomic force microscopy (AFM) and found to be very low (≤ 0.3 nm) and comparable. It is worth noting that the carrier lifetime data presented in this study are based on the average values obtained from lifetime mapping on each sample, with thousands of measured points. The uniformity of the carrier lifetime in each sample is greater than 95%, with 1 mm edge exclusion.

As seen in Fig. 1, sample C exhibits an exceptionally high carrier lifetime compared to the other samples. Furthermore, the samples with intentional nitrogen doping (C and L) exhibit substantially longer carrier lifetimes than unintentionally doped ones (F and L), regardless of the net doping concentration.

Temperature-dependent TRPL is a robust method for extracting information about defect levels impacting the carrier lifetime. Figure 2 shows the temperature-dependent TRPL decay curves from NBE emission for all four samples in the temperature range 291–793 K. As is seen, the carrier lifetime improves at elevated temperatures, whereas this improvement is more than threefold for the samples with relatively shorter RT carrier lifetimes (samples F and D). In contrast, it is only twofold for samples with long RT carrier lifetime (samples C and L).

B. DLTS and MCTS measurements

When performing DLTS measurement on the studied samples, only the $Z_{1/2}$ and $EH_{6/7}$ -related peaks could be observed. Knowing that both relate to the different charge states of V_C in the epitaxial layers,²² the DLTS spectra are provided around the $Z_{1/2}$ peak region for all samples, see Fig. 3(a) ($Z_{1/2}$ peak position at ~ 270 K). Based on measured carrier lifetimes, it is expected that samples with long carrier lifetimes should contain a low concentration of the $Z_{1/2}$ center. However, the calculated values of $Z_{1/2}$ (see Table III) do not differ substantially among different samples and range from 4.7×10^{11} to $1.4 \times 10^{12} \text{ cm}^{-3}$.

Figure 3(b), showing the carrier lifetime as a function of the $Z_{1/2}$ concentration, does not reveal a meaningful correlation between the two parameters. Importantly, sample D exhibits the lowest measured $Z_{1/2}$ concentration, but does not show the highest measured carrier lifetime—instead, the lowest carrier lifetime is observed for the sample with the lowest $Z_{1/2}$ concentration. These results imply that other recombination/trapping mechanisms besides $Z_{1/2}$ are also active and controlling carrier lifetime in the studied epitaxial layers.

The DLTS measurement of an n-type epitaxial layer gives information only on the energy levels in the upper half of the bandgap. To explore the lower half of the bandgap and investigate the presence of minority carrier traps, MCTS measurements were performed on the samples. The typical defect levels observed in as-grown, n-type epitaxial layers through MCTS are the so-called shallow B ($E_V + 0.27$ eV), HS1 ($E_V + 0.35$ eV), and D-center ($E_V + 0.61$ eV).¹⁴ E_V denotes the valence band edge.

Figure 4(a) presents the data obtained from MCTS measurements, where the inset shows zoomed-in MCTS spectra in the temperature range 130–320 K. The intensities of the B-related peaks (B and D) vary strongly across the sample set. The extracted concentrations of the shallow B and D-center in the samples are summarized in Table III. Plots of the defect concentrations vs RT minority carrier lifetimes are depicted in Figs. 4(b) and 4(c).

As demonstrated by Fig. 4(a), shallow B is the dominant defect in all samples. The shallow B concentration was surprisingly high in sample L, whereas sample F had a substantially lower concentration, and samples C and D exhibited even lower concentrations for this defect level. Furthermore, a closer look at the shallow B peak in MCTS spectra (not shown here) revealed that it consists of two or

TABLE III. Deep level concentrations (cm^{-3}) extracted from DLTS and MCTS measurements on the samples.

Sample ID	$Z_{1/2}$	B	D
C	9.5×10^{11}	4.3×10^{12}	5.3×10^{11}
D	4.7×10^{11}	9.7×10^{12}	2.8×10^{12}
F	1.4×10^{12}	1.8×10^{13}	2.3×10^{12}
L	1.2×10^{12}	4.0×10^{13}	1.0×10^{12}

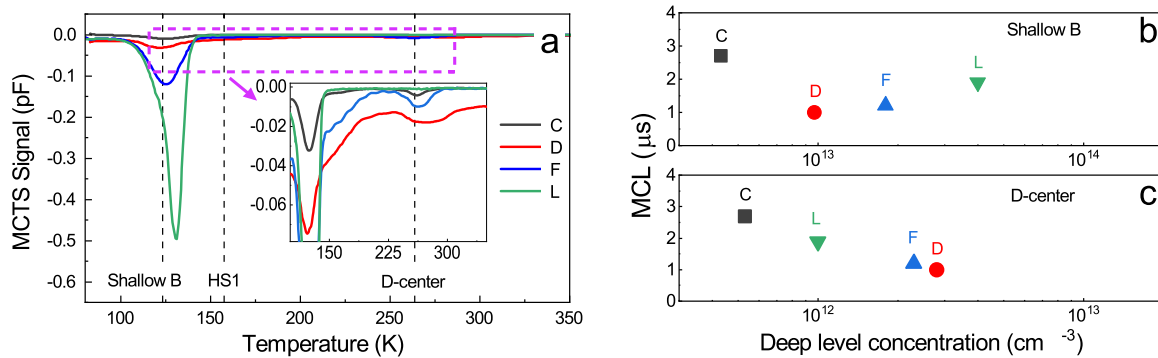


FIG. 4. (a) MCTS spectra taken in the temperature range 80–375 K. The inset is zoomed-in spectra around the D-center-related peak. (b) Measured carrier lifetime vs shallow B concentration, and (c) measured carrier lifetime vs D-center concentrations in the studied samples.

more components; however, the details are out of scope of this paper. For the D-center related peak, samples F and D exhibited higher concentrations, whereas sample C had a five times lower value (see Table III). Regarding the D-center in sample L, a signal was detected around the D-center peak position for some correlation functions only.

A value around $1 \times 10^{12} \text{ cm}^{-3}$ was extracted for the parameter sets where the D-center peak was visible in sample L, and is, therefore, listed in Table III.

In samples with a higher concentration of D-center, the HS1 related peak was also observed. The MCTS results indicate that both the D-center and HS1 deep levels are more pronounced in unintentionally doped samples. By comparing the concentration of shallow B and RT carrier lifetimes [in Fig. 4(b)], no meaningful relationship between these two values is observed. On the other hand, a similar comparison between the concentration of D-center and the RT carrier lifetime for samples C, F, and D shows a clear inverse relationship [see Fig. 4(c)] for all samples. In other words, the minority carrier lifetime in the studied epitaxial layers appears to be correlated with the concentration of the D-center—in clear contrast with common expectations that the $Z_{1/2}$ level is the main defect controlling the carrier lifetime.

C. Temperature-dependent 530 nm TRPL

Temperature-dependent TRPL, at wavelengths other than the NBE range, provides information about different recombination processes at any given specific wavelength.²⁸ MCTS revealed that B-related defects are prominent in the lower half of the bandgap in the studied samples. It is also known that B-related defects in 4H-SiC lead to a broad PL peak around 530 nm.²⁹ Figures 5(a) and 5(b) present recorded 530 nm, TRPL decay spectra for all samples at 296 and 887 K, respectively. The RT decay spectra [Fig. 5(a)] consist of two components, with fast and slow characters. As is shown in the inset, the fast component's slope is larger for samples D and F compared to samples C and L. Furthermore, the slow components' decay constant also differs for different samples. The extracted values are given in Table IV.

From the curves recorded at 887 K [Fig. 5(b)], it becomes clear that the slow components have disappeared, leaving the fast component alone, with an almost similar decay constant of $\sim 1 \mu\text{s}$ for all samples. To explain the significant change in the shape of decay curves at 887 K, the measurement was repeated with smaller temperature intervals. Figure 6 shows 530 nm, TRPL decay curves, recorded in the temperature range 296–870 K for each sample. The slow

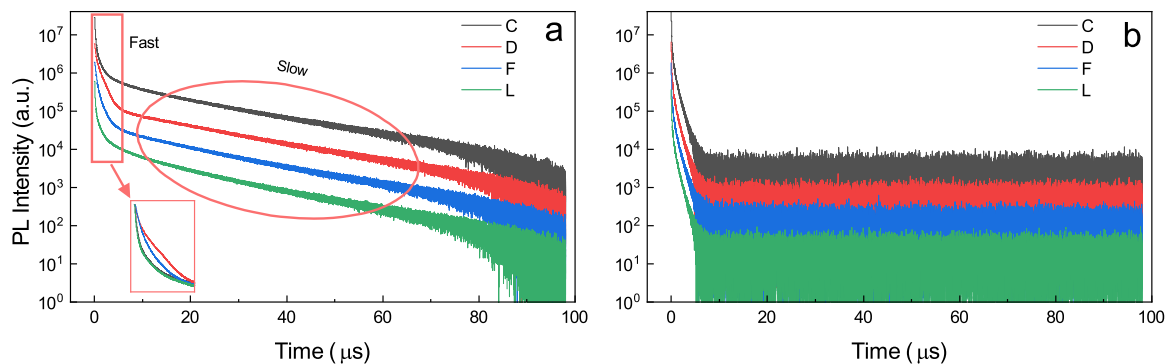


FIG. 5. (a) RT and (b) 887 K TRPL decay curves for all samples recorded at the emission wavelength of 530 nm. The inset in (a) shows the fast decay part of all samples.

TABLE IV. The extracted values of decay constants for the slow component in 530 nm RT TRPL curves.

Sample ID	530 nm slow component decay constant (μs)
C	18.4
D	17.5
F	16.6
L	15.3

component of the decay curve starts to decay faster at temperatures above 350 K. As the temperature is raised above 422 K, the slow component disappears, and at further elevated temperatures (≥ 573 K), only the fast decay component remains. The decay constant for this component remains the same until the last measurement point (887 K).

IV. DISCUSSION

A. Impact of deep levels on charge carrier dynamics

Even though the measured lifetime varies over a wide range in the different samples, i.e., from 1.0 to 2.7 μs , it is important to note that the thickness of each epitaxial layer is only 25 μm . Therefore, even the lowest measured lifetime of 1 μs can be considered high for such a thin layer. In this regard, two possibilities can be considered, to explain the long carrier lifetimes. One is the slow de-

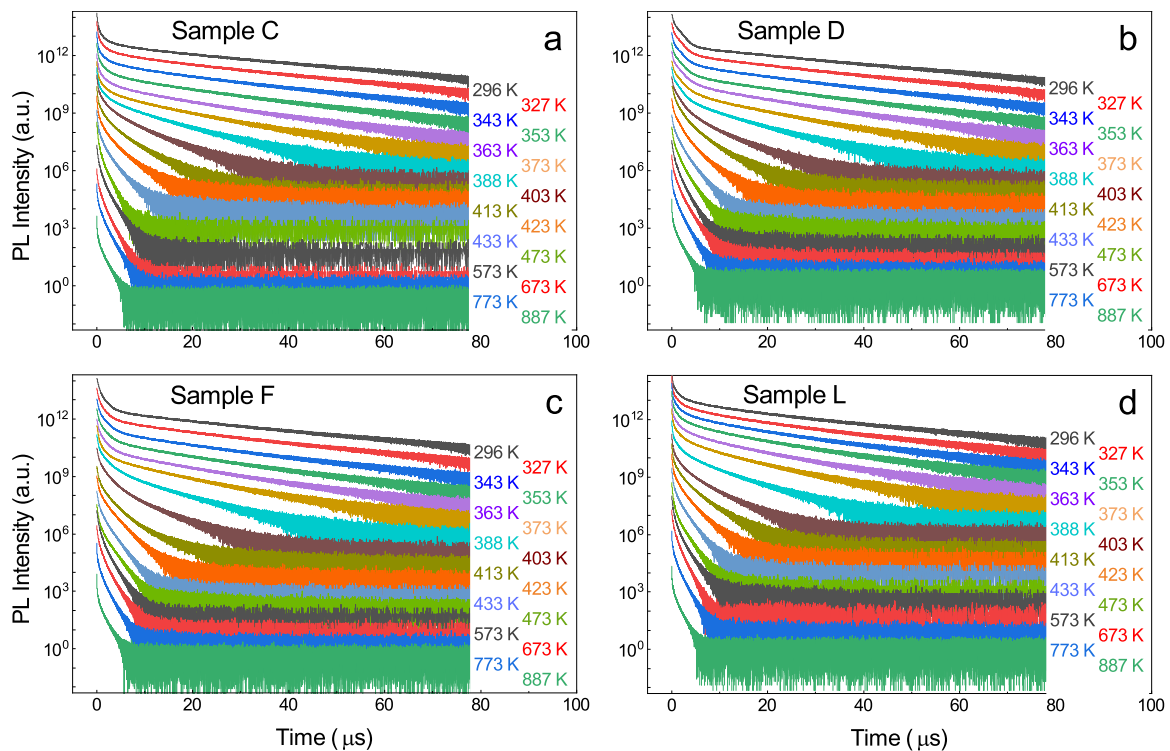
trapping of minority carrier holes in n-type epitaxial layers, which leads to long carrier lifetimes, as reported by Klein *et al.* and Shrivastava *et al.*^{27,30} In this case, the minority-carrier, hole de-trapping centers slowly emit already captured holes into the valence band. In the presence of the majority electrons, they recombine through band-to-band recombination and contribute to the long tail of the NBE photoluminescence decay curve. The decomposition of a single component RT exponential decay into two-component exponential decay of NBE emission in the temperature range 330–450 K is the characteristic of samples containing such centers.²⁷ However, in our samples, only one exponential component was present at all measurement temperatures (Fig. 2), evidencing that the slow de-trapping of minority holes cannot be responsible for the long carrier lifetimes.

The second possible explanation for the long carrier lifetimes is a low concentration of Shockley Read Hall (SRH) recombination centers. The relationship between SRH recombination lifetime and SRH trap concentration is given by

$$\frac{1}{\tau_{\text{SRH}}} = N_{\text{trap}} \times v_t \times \sigma_{\text{trap}}. \quad (1)$$

Here, τ_{trap} , N_{trap} , v_t , and σ_{trap} are the SRH recombination lifetime through a specific trap, trap concentration, the thermal velocity of minority carriers, and the trap's capture cross-section, respectively.

By considering $Z_{1/2}$ as the main lifetime limiting defect and taking the extracted $Z_{1/2}$ densities from DLTS results into account

**FIG. 6.** (a) 530 nm TRPL decays of each sample, recorded in the temperature range 296–887 K, for samples (a) C, (b) D, (c) F, and (d) L.

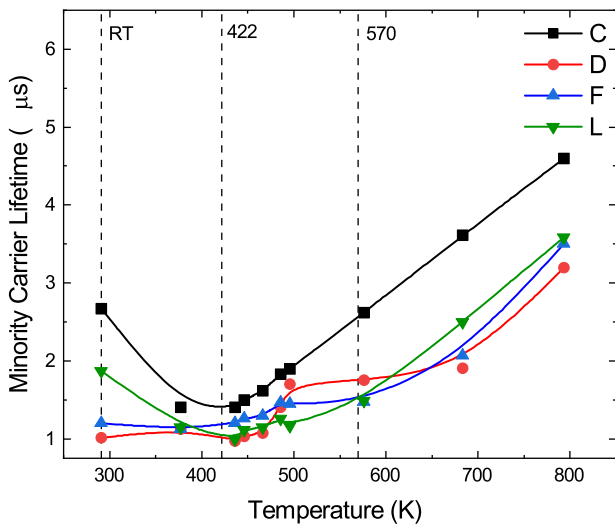


FIG. 7. Extracted carrier lifetimes vs TRPL measurement temperatures from RT to 793 K for all samples. A surging point at 422 K is present in all samples, and another is seen at 570 K only in samples D and F.

[Figs. 3(a) and 3(b)], sample C should exhibit almost half of the carrier lifetime compared to sample D, as the $Z_{1/2}$ concentration in sample C is almost double that of sample D. Correspondingly, samples F and L should have similar carrier lifetime values, as they have similar $Z_{1/2}$ densities. However, in both cases, the measured values of carrier lifetime and $Z_{1/2}$ concentration are not correlated. These deviations imply that the commonly accepted lifetime-limiting defect ($Z_{1/2} \equiv V_C$) in n-type 4H-SiC epitaxial layers cannot alone be responsible for reducing the lifetime in the studied samples, but instead, other defects may also be active in controlling the carrier lifetimes.

Interpreting data obtained from temperature-dependent NBE TRPL helps identify the different mechanisms impacting the minority carrier dynamics and lifetimes. In principle, due to the thermal

energy generated during the measurement, the carriers' depopulation from the deep levels affects the carrier lifetime. Consequently, the influence of the depopulation on the carrier lifetime vs temperature curves must be observed. Figure 7 depicts such a curve for all the studied samples. As can be seen, samples C and L follow a similar pattern, through which their measured carrier lifetime starts to decrease above RT and reaches a minimum at ~ 422 K. With a further increase in temperature, the carrier lifetimes begin to rise almost linearly with temperature. In contrast, samples D and F have either a nearly constant value up to ~ 422 K or show a slight increase in the measured carrier lifetimes. A small increment in carrier lifetime is observed in the temperature range 422–570 K, followed by a near-linear increase with temperature up to 793 K.

The two surging points at ~ 422 K and ~ 570 K are also highlighted in Fig. 7, which means that at least two mechanisms impact the measured carrier lifetimes in the studied samples. The origin of the two mechanisms will be discussed later when the MCTS results and the information extracted from 530 nm temperature-dependent TRPL are also analyzed.

For a better interpretation of the temperature-dependent, 530-nm TRPL curves and their correlation with the concentrations of B-related defects in MCTS spectra, the extracted slow components' decay constants are plotted vs temperature in Fig. 8. As can be seen, the decay constants of all samples start to decrease significantly above room temperature and converge to an almost similar value at temperatures above 422 K. By comparing Figs. 7 and 8(a), it is revealed that the first surging point at 422 K in Fig. 7 can be related to the almost complete elimination of the slow component of the TRPL decay curves at 530 nm, as shown in Fig. 8(a).

Comparing the RT values of Fig. 8(a) (given in Table IV) with the concentration of shallow B obtained from MCTS spectra reveals an inverse relationship between the two values, as shown in Fig. 8(b). However, it is commonly assumed that shallow B is not a recombination center,³¹ thus, not contributing to the luminescence at 530 nm. Therefore, shallow B should not be directly involved in the recombination process that results in the 530 nm TRPL decay. Yang *et al.*²⁸ have reported that the slow component of the 530-nm, TRPL decay curve originates from e-A (free electron to acceptor) recombination, where the acceptor level is shown to be the D-center. Furthermore,

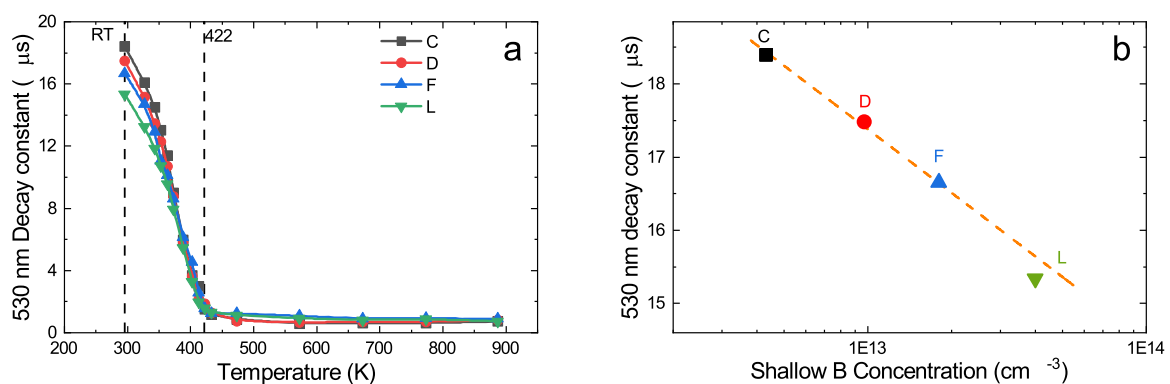


FIG. 8. (a) 530 nm TRPL decay constants vs temperature for all samples. These decay constants converge to a specific value (~ 1 μ s) above 422 K in all samples. (b) Shallow B concentrations in different samples vs their extracted 530 nm decay constant. The solid line is the fitted exponential line to the trend.

they have shown that at higher measurement temperatures (473 K in their report), the decay constant for this component reduces significantly. Similar behavior has been observed in the samples studied herein. As shown in Fig. 8(b), the exponential decay constants for the slow component of the 530-nm, TRPL decay curves quench significantly with temperature in all samples and converge to a value around $1 \mu\text{s}$ at ~ 422 K.

In fact, upon increasing the temperature to 422 K, shallow B, as a minority carrier trap,³¹ is getting depopulated, and the holes start to emit to the valence band. Consequently, the number of available holes for recombination is increased. As a result, the recombination probability for an individual hole decreases and leads to a longer carrier lifetime, assuming a low-injection condition. It should be noted that because of the ionization of N donor atoms, the concentration of free electrons increases at elevated temperatures. Accordingly, the probability of donor–acceptor pair (DAP) recombination decreases. However, as an acceptor level, the D-center can still contribute to the e–A recombination and reduce the carrier lifetime. As a result, the carrier lifetime curves in Fig. 7 grow strikingly for the samples with lower D-center concentrations (samples C and L). In contrast, samples with a relatively higher concentration of D-center (samples D and F) display a flat trend with temperature after a slight initial increase.

In Ref. 28, it was also shown that the fast component of the RT, 530-nm, TRPL decay is related to the D-center concentration. However, at elevated temperatures, the decay constants for DAP and e–A recombination become indistinguishable. Thus, other information from Fig. 6 should be extracted to explain the next surging point for samples D and F at 570 K in Fig. 7.

The area under a TRPL decay curve gives an estimate of the number of recombination events. Figure 9(a) shows the calculated areas under the 530-nm, TRPL decay curves vs temperature for the studied samples. By comparing the 422 K values of the area under the TRPL curve [in Fig. 9(a)] with the concentration of the D-center [Fig. 4(c)] for each sample, it was found that there is

a linear relationship between the D-center concentration and the number of recombination events at 530 nm [Fig. 9(b)]. It should be noted that the RT values of the decay areas could not be used here, as it was already shown that shallow B can significantly affect the obtained information from TRPL at temperatures below ~ 422 K. Differently said, in the samples with a higher D-center concentration, the minority carriers tend to recombine at 530 nm. Eventually, the number of available minority carriers to recombine at NBE decreases. With the presence of excess majority carriers, the recombination probability increases and results in a lower carrier lifetime. It is evident that increasing the temperature from RT significantly reduces the number of recombination events occurring at 530 nm. Consequently, fewer minority carriers are disappearing through this recombination center and, thus, are available for recombination through NBE emission. At temperatures above 700 K, all the curves converge to a similar value, implying the neutralization of the D-center's effect on the carrier lifetime above this temperature. Figure 9(a) further reveals that the area under TRPL decay curves for all samples reduces beyond 570 K. A comparison among Figs. 7, 9(a), and 9(b) indicates that the neutralization of the D-center at ~ 570 K leads to a substantial reduction of the recombination at 530 nm. Consequently, a linear increment in the measured carrier lifetimes above this temperature is observed.

The relationship shown in Fig. 9(b) can also be extended to the HS1 defect level. However, it is known that HS1 is related to the L1 line at ~ 420 nm in PL of 4H–SiC³² and, thus, not contributing to the 530-nm TRPL decay.

Comparing the curves of samples C and L in Fig. 9(a) shows that at a temperature of ~ 422 K, where all the curves are becoming flat, the curve for sample L climbs over that of sample C and continues with a higher value until the curves again merge at ~ 570 K. This behavior could be explained by a relatively higher concentration of shallow B for sample L than sample C, as obtained from MCTS spectra. It was shown that above ~ 422 K, shallow B hole traps start to emit holes to the valence band. As a result, the number of available holes

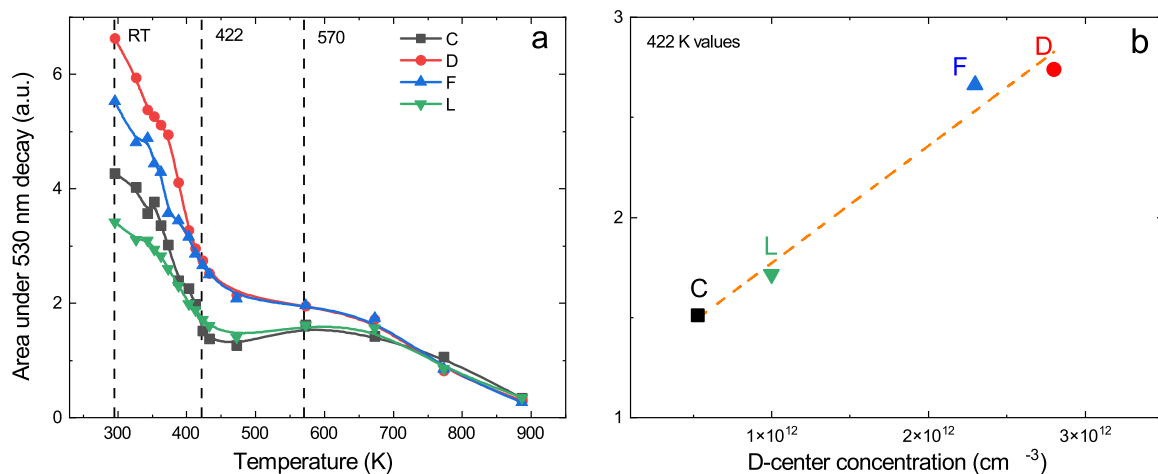


FIG. 9. (a) Integrated decay area vs temperature extracted from 530-nm, TRPL decay curves at different temperatures for all samples, and (b) calculated 530-nm, TRPL decay area at 422 K vs D-center concentration.

for recombination increases. As this increment is relatively higher in sample L than in sample C and also considering a slightly higher concentration of the D-center in sample L, more recombination events are expected to occur at 530 nm in sample L at temperatures above ~422 K.

Regarding the plateau between 422 and 570 K in Fig. 9(a), it should be noted that, upon de-trapping of minority holes from the shallow B level, the 530-nm decay gets accelerated by an increase in the number of available holes in the valence band. On the other hand, the neutralization of the D-center and the increased number of free electrons at higher temperatures oppose the accelerated 530-nm decay, resulting in a flat curve between 422 and 570 K in Fig. 9(a).

B. Influence of the growth parameters on B-related deep levels and minority carrier lifetime

As summarized in Table I, all the samples were grown under similar growth conditions, except for the C/Si ratio and growth temperature. Furthermore, two samples (C and L) were doped intentionally, by introducing nitrogen during the epitaxial growth. The other two (samples D and F) were unintentionally doped with residual nitrogen inside the reactor.

TRPL data and MCTS spectra revealed that the main impurity which is limiting carrier lifetime in the studied samples is B, which forms two main defect levels in 4H-SiC: shallow B and D-center. By comparing the extracted concentrations of shallow B for different samples, it is observed that the incorporation of shallow B is relatively higher in samples with relatively lower doping concentrations, independent of intentional or unintentional nitrogen doping. However, the relatively higher incorporation of shallow B in sample L can be explained by considering this sample's somewhat higher C/Si ratio. The main source of unintentional B in CVD-grown layers is graphite, and the partial pressure of B can be considered constant for a fixed growth temperature. However, the incorporation of B in the epitaxial layer may be significantly influenced by the C/Si ratio, following the so-called site competition. As the prominent model for shallow B is B_{Si} ,³³ the formation of this defect is more favored in a C-rich environment. This explanation can be further expanded to the D-center with possible B_C configuration,^{34,35} where the C-rich environment hinders substitution of B on the C site. On the other hand, when considering the $B_{Si}-V_C$ configuration as another proposed model for the D-center,³³ and the explanation for the formation of shallow B, it can be understood that the probability of having $B_{Si}-V_C$ is low, as most of the B_{Si} defects are already bonded to C atoms. However, the higher $Z_{1/2}$ concentration in sample L could explain the reason for having a higher D-center concentration in this sample. Furthermore, it is also known that the incorporation of B is further enhanced at low growth temperatures.¹⁴ Thus, the D-center formation is further pronounced in samples grown at relatively low temperatures and with a low C/Si ratio (sample D).

V. CONCLUSION

A significantly high charge carrier lifetime was obtained in 25- μm -thick, 4H-SiC epitaxial layers; however, it varied over a wide range of 1.0–2.7 μs . The samples were grown under similar growth conditions, except for the growth temperature, C/Si ratio, and N

doping. A relatively high carrier lifetime was observed in samples grown with intentional N doping compared to unintentionally doped samples, regardless of doping concentration, as long as it was less than $2 \times 10^{14} \text{ cm}^{-3}$. Slow de-trapping of minority holes from minority carrier traps was discounted as the reason for the observed behavior. A low concentration of $Z_{1/2}$ defects is observed in all samples, but no meaningful correlation was found between the $Z_{1/2}$ concentration and charge carrier lifetime, indicating that other defects might be active in controlling the charge carrier lifetime in these samples. MCTS measurements revealed the presence of B-related defect levels; shallow B and D-center. Analysis of TRPL data (temperature-dependent NBE and at 530 nm) and their comparison with DLTS and MCTS results indicate that B-related defects in the epitaxial layer are effectively controlling the minority carrier dynamics. Temperature-dependent TRPL measurements in the NBE and at 530-nm spectral ranges reveal that although shallow B is not a recombination center, with trapping and de-trapping of minority holes, it can significantly impact the RT minority carrier lifetime. Comparison of MCTS and TRPL data shows a one-to-one correlation between the D-center concentration and charge carrier lifetime, indicating that B-related impurities are probably the main lifetime killer when $Z_{1/2}$ concentration is very low. The main source of B in SiC epitaxial layers is the graphite parts of the CVD reactor, which act as a continuous source of unintentional B doping. We have observed that the combination of intentional N doping and a C-rich environment suppresses the formation of the D-center; however, the latter pronounces the shallow B incorporation in the epitaxial layers.

ACKNOWLEDGMENTS

The financial support from the Swedish Energy Agency Energimyndigheten Project Nos. 43611-1 and 45398-1 and Swedish Research Council VR Grant No. 2020-05444 is acknowledged. The work of M.E.B. was supported by an ETH Zurich Postdoctoral Fellowship. Financial support was also provided by the Research Council of Norway through the FRIPRO project, QuTe (Grant No. 325573), and the Norwegian Micro- and Nano-Fabrication Facility, NorFab, Project No. 295864.

AUTHOR DECLARATIONS

Conflict of Interest

The authors have no conflicts to disclose.

Author Contributions

Misagh Ghezellou: Conceptualization (equal); Data curation (lead); Formal analysis (lead); Investigation (lead); Methodology (equal); Validation (lead); Visualization (lead); Writing – original draft (lead). **Piyush Kumar:** Formal analysis (supporting), Validation (supporting). **Marianne E. Bathen:** Formal analysis (supporting); Validation (supporting); Writing – review & editing (supporting). **Robert Karsthof:** Formal analysis (supporting); Validation (supporting). **Einar Ö. Sveinbjörnsson:** Conceptualization (equal); Methodology (equal); Supervision (supporting). **Ulrike Grossner:** Formal analysis (supporting); Resources (supporting); supervi-

sion (supporting). **J. Peder Bergman**: Conceptualization (equal); Methodology (supporting); Resources (supporting); supervision (supporting). **Lasse Vines**: Formal analysis (supporting); Resources (supporting); supervision (supporting). **Jawad Ul-Hassan**: Conceptualization (equal); Formal analysis (supporting); Funding acquisition (lead); Methodology (equal); Project administration (lead); Resources (lead); Supervision (lead); Validation (equal); Writing – review & editing (lead)

DATA AVAILABILITY

The data that support the findings of this study are available from the corresponding author upon reasonable request.

REFERENCES

- 1 T. Kimoto and Y. Yonezawa, “Current status and perspectives of ultrahigh-voltage SiC power devices,” *Mater. Sci. Semicond. Process.* **78**, 43–56 (2018).
- 2 M. Imaizumi and N. Miura, “Characteristics of 600, 1200, and 3300 V planar SiC-MOSFETs for energy conversion applications,” *IEEE Trans. Electron Devices* **62**, 390–395 (2015).
- 3 N. Kaji, J. Suda, and T. Kimoto, *Jpn. J. Appl. Phys.* **54**, 098004 (2015).
- 4 J. ul Hassan, H. T. Bae, L. Lilja, I. Farkas, I. Kim, P. Stenberg, J. W. Sun, O. Kordina, P. Bergman, S. Y. Ha, and E. Janzén, *Mater. Sci. Forum* **778–780**, 179–182 (2014).
- 5 H. Pedersen, S. Leone, A. Henry, F. C. Beyer, V. Darakchieva, and E. Janzén, “Very high growth rate of 4H–SiC epilayers using the chlorinated precursor methyltrichlorosilane (MTS),” *J. Cryst. Growth* **307**, 334–340 (2007).
- 6 F. La Via, G. Galvagno, G. Foti, M. Mauceri, S. Leone, G. Pistone, G. Abbondanza, A. Veneroni, M. Masi, G. Valente, and D. Crippa, “4H–SiC epitaxial growth with chlorine addition,” *Chem. Vap. Deposition* **12**, 509–515 (2006).
- 7 S. Leone, A. Henry, E. Janzén, and S. Nishizawa, *J. Cryst. Growth* **362**, 170–173 (2013).
- 8 N. A. Mahadik, R. E. Stahlbush, and W. Sung, “Formation mechanism of horizontal-half-loop arrays and stacking fault expansion behavior in thick SiC epitaxial layers,” *J. Appl. Phys.* **131**, 225702 (2022).
- 9 L. X. Zhao, L. Yang, and H. W. Wu, “High quality 4H–SiC homo-epitaxial wafer using the optimal C/Si ratio,” *J. Cryst. Growth* **530**, 125302 (2020).
- 10 M. Yazdanfar, I. G. Ivanov, H. Pedersen, O. Kordina, and E. Janzén, “Reduction of structural defects in thick 4H–SiC epitaxial layers grown on 4° off-axis substrates,” *J. Appl. Phys.* **113**, 223502 (2013).
- 11 A. Salemi, H. Elahipanah, B. Buono, A. Hallén, J. U. Hassan, P. Bergman, G. Malm, C.-M. Zetterling, and M. Östling, “Conductivity modulated on-axis 4H–SiC 10+ kV PiN diodes,” in *2015 IEEE 27th International Symposium on Power Semiconductor Devices and IC’s (ISPSD)* (IEEE, 2015), pp. 269–272.
- 12 A. B. Renz, O. J. Vavasour, A. Pérez-Tomás, Q. Z. Cao, V. A. Shah, Y. Bonyadi, V. Pathirana, T. Trajkovic, G. W. C. Baker, P. A. Mawby, and P. M. Gammon, *Mater. Sci. Forum* **1062**, 190–194 (2022).
- 13 H. Lee, V. Smet, and R. Tummala, *IEEE J. Emerging Sel. Top. Power Electron.* **8**, 239–255 (2020).
- 14 J. Zhang, L. Storasta, J. P. Bergman, N. T. Son, and E. Janzén, *J. Appl. Phys.* **93**, 4708–4714 (2003).
- 15 T. Kimoto, T. Hiyoshi, T. Hayashi, and J. Suda, *J. Appl. Phys.* **108**, 083721 (2010).
- 16 I. D. Booker, J. U. Hassan, L. Lilja, F. C. Beyer, R. Karhu, J. P. Bergman, Ö. Danielsson, O. Kordina, E. Ö. Sveinbjörnsson, and E. Janzén, *Cryst. Growth Des.* **14**, 4104–4110 (2014).
- 17 T. Kimoto, Y. Nanen, T. Hayashi, and J. Suda, *Appl. Phys. Express* **3**, 121201 (2010).
- 18 H. M. Ayedh, R. Nipoti, A. Hallén, and B. G. Svensson, “Elimination of carbon vacancies in 4H–SiC employing thermodynamic equilibrium conditions at moderate temperatures,” *Appl. Phys. Lett.* **107**, 252102 (2015).
- 19 J. Hassan and J. P. Bergman, *J. Appl. Phys.* **105**, 123518 (2009).
- 20 P. B. Klein, B. V. Shanabrook, S. W. Huh, A. Y. Polyakov, M. Skowronski, J. J. Sumakeris, and M. J. O’Loughlin, *Appl. Phys. Lett.* **88**, 052110 (2006).
- 21 K. Danno, D. Nakamura, and T. Kimoto, *Appl. Phys. Lett.* **90**, 202109 (2007).
- 22 N. T. Son, X. T. Trinh, L. S. Løvlie, B. G. Svensson, K. Kawahara, J. Suda, T. Kimoto, T. Umeda, J. Isoya, T. Makino, T. Ohshima, and E. Janzén, “Negative-U system of carbon vacancy in 4H–SiC,” *Phys. Rev. Lett.* **109**, 187603 (2012).
- 23 L. Lilja, I. D. Booker, J. ul Hassan, E. Janzén, and J. P. Bergman, *J. Cryst. Growth* **381**, 43–50 (2013).
- 24 T. Hiyoshi and T. Kimoto, “Elimination of the major deep levels in n- and p-type 4H–SiC by two-step thermal treatment,” *Appl. Phys. Express* **2**, 091101 (2009).
- 25 L. Storasta, H. Tsuchida, T. Miyazawa, and T. Ohshima, “Enhanced annealing of the $Z_{1/2}$ defect in 4H–SiC epilayers,” *J. Appl. Phys.* **103**, 013705 (2008).
- 26 S. Weiss and R. Kassing, “Deep level transient fourier spectroscopy (DLTFS)—A technique for the analysis of deep level properties,” *Solid-State Electron.* **31**, 1733–1742 (1988).
- 27 P. B. Klein, A. Shrivastava, and T. S. Sudarshan, *Phys. Status Solidi A* **208**, 2790–2795 (2011).
- 28 A. Yang, K. Murata, T. Miyazawa, T. Tawara, and H. Tsuchida, *J. Phys. D: Appl. Phys.* **52**, 10LT01 (2019).
- 29 M. Ikeda, H. Matsunami, and T. Tanaka, *Phys. Rev. B* **22**, 2842–2854 (1980).
- 30 A. Shrivastava, P. B. Klein, E. R. Glaser, J. D. Caldwell, A. V. Bolotnikov, and T. S. Sudarshan, “Long carrier lifetime in 4H–SiC epilayers using chlorinated precursors,” *Mater. Sci. Forum* **615–617**, 291–294 (2009).
- 31 I. D. Booker, “Carrier lifetime relevant deep levels in SiC,” Ph.D. thesis, Linköping University, Semiconductor Materials, Faculty of Science and Engineering, 2015.
- 32 L. Storasta, F. H. C. Carlsson, S. G. Sridhara, J. P. Bergman, A. Henry, T. Egilsson, A. Hallén, and E. Janzén, “Pseudodonor nature of the D_1 defect in 4H–SiC,” *Appl. Phys. Lett.* **78**, 46–48 (2001).
- 33 T. Troffer, M. Schadt, T. Frank, H. Itoh, G. Pensl, J. Heindl, H. P. Strunk, and M. Maier, *Phys. Status Solidi A* **162**, 277–298 (1997).
- 34 I. Capan, Y. Yamazaki, Y. Oki, T. Brodar, T. Makino, and T. Ohshima, “Minority carrier trap in n-type 4H–SiC Schottky barrier diodes,” *Crystals* **9**, 328 (2019).
- 35 V. J. B. Torres, I. Capan, and J. Coutinho, “Theory of shallow and deep boron defects in 4H–SiC,” *Phys. Rev. B* **106**, 224112 (2022).